

Single-phase and correlated-phase estimation with multiphoton annihilated squeezed vacuum states: An energy-balancing scenario

N. Samantaray,^{1,*} I. Ruo-Berchera,² and I. P. Degiovanni^{2,3}

¹*Quantum Engineering Technology Labs, H. H. Wills Physics Laboratory and Department of Electrical and Electronic Engineering, University of Bristol, Bristol BS8 1FD, United Kingdom*

²*INRIM, Strada delle Cacce 91, I-10135 Torino, Italy*

³*INFN, via P. Giuria 1, I-10125 Torino, Italy*



(Received 25 November 2019; accepted 27 April 2020; published 4 June 2020)

In recent years, several works have demonstrated the advantage of photon-subtracted Gaussian states for various quantum optics and information protocols. In most of these works, the relation between the advantages and the usual increasing energy of the quantum state related to photon subtraction was not clearly investigated. In this paper, we study the performance of an interferometer injected with multiphoton-annihilated squeezed vacuum states mixed with coherent states for both single- and correlated-phase estimations. For single-phase estimation, although the use of multiphoton-annihilated squeezed vacuum states at low mean photons per mode provides an advantage compared to classical strategy, when the total input energy is held fixed, the advantage due to photon subtraction is completely lost. However, for the correlated case in the analogous scenario, some advantage appears to come from both the energy rise and improvement in photon statistics. In particular quantum enhanced sensitivity with photon-subtracted states appears more robust to losses, showing an advantage of about 30% with respect to the squeezed vacuum state in the case of a realistic value of the detection efficiency.

DOI: [10.1103/PhysRevA.101.063810](https://doi.org/10.1103/PhysRevA.101.063810)

I. INTRODUCTION

Non-Gaussian states have been recognized as a valuable resource for many quantum information processing protocols [1], for example, for enhancing the fidelity of quantum teleportation [2–5], for improving the secret key rate in quantum key distribution [6,7], and in quantum cloning of coherent states [8]. These exotic states are required in Gaussian entanglement distillation [9–11], error correction [12], noiseless amplification [13,14], and fundamental loophole-free Bell tests in continuous variables [15,16]. More recently, resource theories quantifying the importance of Wigner negativity and non-Gaussianity for continuous-variable quantum computation have been reported [17,18]. Because of the higher potential distinguishability of non-Gaussian states from their original Gaussian states, they have proven useful for more precise parameter estimation in quantum optics [19,20]. Photon addition or photon subtraction can transform a Gaussian in a non-Gaussian state [21–23]. Agarwal and Tara [24] were the first to propose the transformation of a classical-like coherent state into a nonclassical state through photon addition, and this operation was experimentally implemented for the first time for coherent and thermal states in [25,26]. Furthermore, photon addition and subtraction have been reported to enhance the entanglement in the two-mode squeezed vacuum state (TSV) [27–29]. It is well known that each mode of the TSV has super-Poissonian photon statistics. In an experimental work [30], it was reported that multiphoton subtraction makes the TSV less noisy and helps in shifting the most

probable distribution to a higher mean photon number, thereby increasing the mean energy of the resulting state. In recent years, photon-subtracted TSV states have been theoretically investigated for other applications; for example, in [31] these states were proved to be advantageous with respect to TSVs for target detection in a noisy environment, a scheme dubbed “quantum illumination” [32,33]. Their advantage has also been demonstrated in single interferometry with parity measurements [20,34,35].

Since the seminal work by Caves [36], it has been well known that a single-mode squeezed vacuum (SSV) mixed with an intense coherent state provides a substantial advantage in practical phase estimation, and very recently, that scheme was applied by the LIGO and VIRGO collaborations to further improve the sensitivity of gravitational wave detectors [37,38]. It has also been shown that a squeezed vacuum mixed with an intense coherent beam allows us to approach the optimal sensitivity achievable by a linear interferometer operated with a large photon number and non-negligible losses [39]. In that context, a single-photon subtracted SSV has an advantage in phase estimation and allows us to reach Heisenberg’s limit [40]. In that case [40], the mean energy increase of the photon-subtracted state is compensated by a reduction of the coherent beam energy in order to keep constant the total input photon number. Photon-subtracted SSVs mixed with coherent states lead to improved phase-shift sensitivity in the parity measurement [34]. In this work, because of the nonlinear increase of the mean number of photons with the number of subtracted photons, the total average number of photons is fixed by choosing a fixed squeezing parameter and increasing coherent energy. This approach is little different from the energy-balancing scenario reported in [40].

*ns17363@bristol.ac.uk

However, in most of the literature with a few exceptions that we will point out later [20,41], it was not clear whether the advantages come from energy shifts of the photon-subtracted states or from their potentially improved photon noise properties. In fact, most of the time, the comparison between the performance of Gaussian quantum states and the corresponding photon-subtracted states has been considered for a fixed squeezed parameter, which means generally that the energy put into the quantum resource is not fixed. Photon subtraction is a complex operation that can be experimentally realized probabilistically or with low efficiency [42]. So if the advantage comes mainly from the increased energy, it could be practically more convenient to increase the squeezing parameter of the Gaussian state, rather than performing photon subtraction. This is the reason why we consider understanding whether the advantage relies solely on an increase of the energy or there are more fundamental reasons that justify the operation such as photon subtraction to be of great importance. Answering this question is the main motivation of this paper.

Specifically, given the importance of practical interferometry [39], here we study in detail multiphoton-subtracted single-mode and two-mode squeezed vacuum states for single-phase and correlated-phase estimation, respectively, by combining them with coherent states on a beam splitter. On the one hand, we show that a multiphoton-subtracted (one-) two-mode squeezed states is formally equivalent to a state obtained by a (one-) two-mode squeezing operator applied to a certain class of finite superposition states in the photon-number basis. This class of states was investigated earlier [43,44], and these states show quadrature squeezing. One could expect that this initial squeezing could bring a benefit in phase estimation. We have therefore investigated this possibility.

In order to properly understand the origin of the improvement in phase measurement uncertainties, if any, we think that the proper procedure requires that the total energy should be fixed by balancing the energies of the subtracted and unsubtracted states while keeping the coherent pump energy constant. We will consider this energy-balancing condition for both single- and correlated-phase estimations. Similar analysis was done in [20], where an advantage in phase estimation with parity measurement at fixed energy was reported, but that scheme does not involve the mixing with a coherent state, and parity measurement is quite far from realistic applications. In [41], while a precise comparison with two-mode squeezed states with the same energy was not carried out, the authors showed that the larger the ‘‘affinity’’ of a non-Gaussian state with a two-mode squeezed vacuum (with larger energy) is, the larger the teleportation fidelity is.

This paper is organized as follows. In Sec. II, we introduce the multiphoton annihilated single-mode squeezed vacuum (PASSV), discussing its properties and its usefulness, for single-phase estimation by the conventional measurement strategy (Sec. II A) and in the more general framework of the Fisher information (Sec. II B). In Sec. III, we describe the multiphoton symmetrically annihilated two-mode squeezed vacuum (SPATSV) state. In particular, in Sec. III A, we analyze the squeezing and photon statistical properties of SPATSV. In Sec. III B we study the problem of correlated phase estimation. We present results for up to four- and

three-photon subtraction for single- and correlated-phase estimations, respectively. Finally, we summarize and discuss the main results in Sec. IV.

II. PASSVS

PASSV states are defined as

$$|\Psi_{\text{PASSV}}^{(m)}\rangle = N_-^m(\lambda)\hat{a}^m\hat{S}(\lambda e^{i\chi})|0\rangle, \quad (1)$$

where $\hat{S}(re^{i\chi}) = e^{re^{i\chi}a^2 - \text{H.c.}}$ is the single-mode squeezing operator, with r being the squeezing parameter, and χ is the squeezing angle. The squeezing operator applied to the vacuum state originates SSV with energy (mean number of photons) equal to $\lambda = \sinh^2 r$. The number of subtracted photons is m , obtained by m consecutive actions of the annihilation operator \hat{a} . Since photon subtraction is not a unitary operation, it is necessary to introduce the normalization constant $N_-^m(\lambda)$. Its explicit form is $N_-^m(\lambda) = m!(-i\sqrt{\lambda})^m P_m(i\sqrt{\lambda})$ [45], with P_m being the m th-order Legendre polynomial. A known effect of photon subtraction is the increasing of the mean energy of the state. This is intuitively explained because it is more likely to subtract a photon from a highly populated state corresponding to a selection of the more energetic components of the state. For example, the mean photon number of the PASSV state $\mathcal{N}_m(\lambda)$ for $m = 0-3$, which correspond to zero-, one-, two-, and three-photon subtraction from the SSV state, becomes $\mathcal{N}_0 = \lambda$, $\mathcal{N}_1 = 3\lambda + 1$, $\mathcal{N}_2 = 3\lambda(3 + 5\lambda)/(1 + 3\lambda)$, and $\mathcal{N}_3 = (3 + 30\lambda + 35\lambda^2)/(3 + 5\lambda)$, respectively.

We have found a representation for PASSV states (exploiting integration within an ordered product (IWOP) technique [46]) which is equivalent to seeding the squeezing operator with a photon-number superposition state $|\Theta_{(m)}^s(\lambda, \chi)\rangle$ in the input as follows:

$$\begin{aligned} |\Psi_{\text{PASSV}}^{(m)}\rangle &= \hat{S}|\Theta_{(m)}^s(\lambda, \chi)\rangle, \\ |\Theta_{(m)}^s(\lambda, \chi)\rangle &= N_-^m(\lambda)m!(e^{i\chi}\sqrt{\lambda})^m \sum_{l=0}^{[m/2]} \frac{1}{l!\sqrt{(m-2l)!}} \\ &\quad \times \left(\frac{e^{-i\chi}}{2}\sqrt{\frac{1+\lambda}{\lambda}}\right)^l |m-2l\rangle, \end{aligned} \quad (2)$$

where the upper bound of the summation $[m/2]$ stands for the integer part of $m/2$. Without any loss of generality, hereinafter, we set the squeezing angle to $\chi = 0$. For $m = 0$, the input simplifies to the vacuum state, as expected. For $m = 1$, it becomes a single-photon state, as reported in [40]. Note that, for other values of m , it becomes a $[(m+1)/2]$ -component superposition state for odd m and a $[(m+2)/2]$ -component superposition state for even m . The energy increasing with m of the PASSV state can now be understood in terms of an increase of the mean number of photons of the seeding states. The states $|\Theta_{(m)}^s(\lambda, \chi)\rangle$ are known to show quadrature squeezing [43,44], even though they cannot be obtained by any unitary transformation on the vacuum state, like a standard squeezed state. However, these states do not always have lower quadrature noise compared to the vacuum state. In particular, for $m = 1$, the state $|\Theta_{(1)}^s(\lambda, \chi)\rangle$ is a single-photon state with more quadrature noise than the vacuum state. We

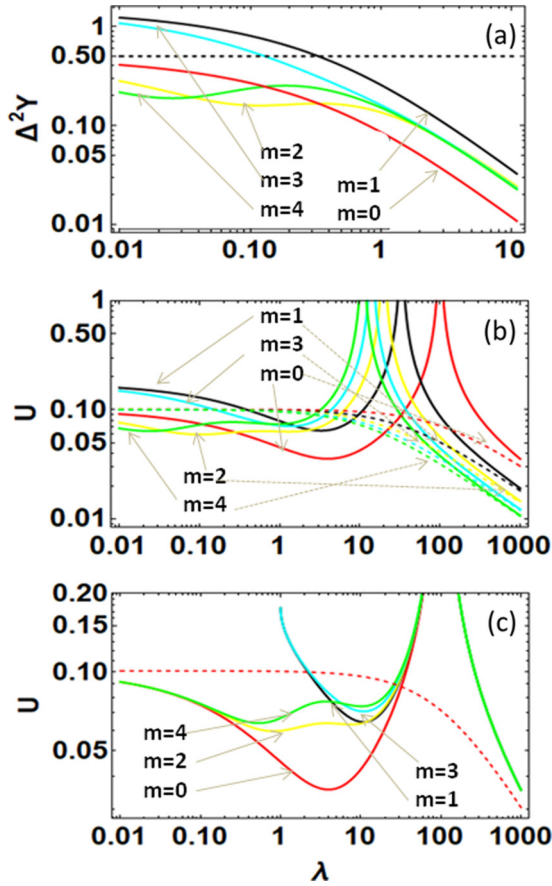


FIG. 1. Quadrature squeezing of PASSV states and phase measurement uncertainty at working point $\phi = \pi/2$ with $\mu = 100$, $\eta = 0.98$, and $\psi = 0$ for different numbers of photon subtraction m : $m = 0$ (solid red line), $m = 1$ (solid black line), $m = 2$ (solid yellow line), $m = 3$ (solid cyan line), and $m = 4$ (solid green line). Dashed lines represent the coherent state: (a) Quadrature squeezing, (b) phase uncertainty, and (c) phase measurement in energy balancing condition.

checked for subsequent odd values of m that although the quadrature noise of the seeding states decreases with respect to the single-photon state, its value still remains above the vacuum noise. This can be appreciated in Fig. 1(a) when considering a small value of the squeezing parameter, which actually means $\hat{S} \approx \mathbb{I}$, with \mathbb{I} being the identity operator. In fact, in Fig. 1 we plot the variance of the quadrature $\hat{Y} = (\hat{a} - \hat{a}^\dagger)/i\sqrt{2}$ of the PASSV states in Eq. (2). In general, we observe that for odd values of m the quadrature noise of the PASSV state is worse than that of the SSV (corresponding to PASSV with $m = 0$), while for even values of m the quadrature noise is better than SSV for low values of λ . Detectors are not ideal in realistic scenarios. The effect of a nonunit quantum efficiency η can be modeled as the evolution of the input field passing through a beam splitter (BS) with transmission equal to η , while the other free port of the BS is in the vacuum state [47]. This approach has been used throughout the paper to account for the optical and detection losses.

In the next section, we will discuss the performance of PASSV states in phase estimation in connection to the quadrature squeezing.

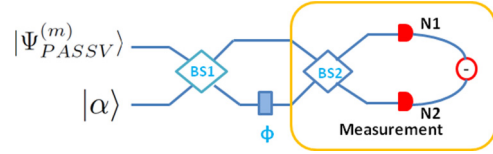


FIG. 2. Schematic of mixing single-mode squeezed vacuum and coherent states in a Mach-Zehnder interferometer for phase estimation ϕ .

A. Single-phase estimation with PASSV states

Let us consider the Mach-Zehnder interferometer (MZI) sketched in Fig. 2, where one port of the first beam splitter is injected with coherent light and the other port is injected with a PASSV state. Thus, the total input state is $|\Psi\rangle_{1,2} = |\Psi_{\text{PASSV}}^{(m)}\rangle \otimes |\alpha\rangle_2$, with $\alpha = |\alpha|e^{i\psi}$, where $|\alpha|$ ($\mu = |\alpha|^2$) and ψ are the amplitude, and phase of the coherent pump. $\mu = |\alpha|^2$ is the mean photon number.

The uncertainty in measuring the phase ϕ in the configuration in Fig. 2 is expressed as

$$U(\phi) = \frac{\sqrt{\Delta^2 \hat{\delta}}}{\left| \frac{\partial \langle \hat{\delta} \rangle}{\partial \phi} \right|}, \quad (3)$$

where $\hat{\delta}$ is the photon-number difference operator at the output port of the interferometer and $\Delta^2 \hat{\delta}$ is its variance. For a zero-mean quadrature field such as SSV, $\langle \hat{\delta} \rangle = (\mu - \lambda) \cos(\phi)$. For SSV, it can be shown that the lowest uncertainty is reached for $\phi = \pi/2$, and in the limit of $\lambda \gg \mu$, the uncertainty is shot noise limited, scaling as $\lambda^{-1/2}$. However, in the case with $\lambda \ll \mu$, the uncertainty is $U(\phi) = (\Delta^2 \hat{X}_{\theta=\psi+\pi/2} / \mu)^{1/2}$, proportional to the noise of the rotated quadrature $\hat{X}_{\theta=\psi+\pi/2} = (\hat{a}e^{-i\theta} + \hat{a}^\dagger e^{i\theta})/\sqrt{2}$. In our case and for the choice of $\psi = 0$, the sub-shot-noise sensitivity is related to the squeezing of the $X_{\pi/2} \equiv Y$ quadrature. For the sake of completeness we mention that for a more specific repartition of the total energy ($\mu + \lambda$) between squeezing and coherent input states, a more efficient scaling of the uncertainty can be achieved [$\propto (\mu + \lambda)^{-3/4}$] [48], and a different, more sophisticated detection scheme could allow us to approach the Heisenberg limit in an ideal decoherence-free scenario [49].

We have derived analytically the uncertainty of the phase estimation according to Eq. (3) when PASSV states are injected. The results are shown graphically in Fig. 1(b), compared with the shot-noise limit (SNL) at the equivalent total energy (dotted lines). The latter is obtained by considering the performance of a coherent state with a mean number of photons equal to the sum of μ and the mean number of photons of the PASSV state, which varies with m . It is easy to check that for PASSV the uncertainty always approaches asymptotically the SNL when $\lambda \gg \mu$. For $\lambda \ll \mu$, the uncertainty is basically determined by the variance of the Y quadrature, reported in Fig. 1(a), as expected. Indeed, the advantage over the SNL is present only in the region of quadrature squeezing, and PASSV ($m > 0$) performs better than SSV only for even m . However, we are going to show that this apparent improvement is due to only the energy increase of the state due to photon subtraction. For that purpose, we have renormalized the energy of the initial SSV state before the photon subtraction,

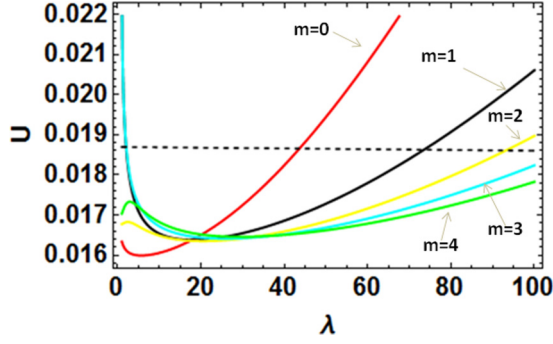


FIG. 3. Phase measurement uncertainty in the energy-balancing scenario for $\phi \neq \pi/2 \approx \pi/2 - 1$, with $\mu = 10000$ and $\eta = 0.98$ for different numbers of photon subtraction m : $m = 0$ (solid red line), $m = 1$ (solid black line), $m = 2$ (solid yellow line), $m = 3$ (solid cyan line), and $m = 4$ (solid green line). The dotted line is the classical strategy.

so that the mean numbers of photons of the subtracted states ($m = 0-4$) are all equal to λ . In this way, also the total input energies to the interferometer are fixed to $N_{\text{tot}} = \mu + \lambda$. With the energy balancing, SSV outperforms PASSV regardless of the values of λ , as presented in Fig. 1(c).

The diverging behavior of uncertainty in Figs. 1(b) and 1(c) for $\lambda = 100$ comes from the singularity in the denominator of Eq. (3), that is, when the mean number of photons of the PASSV state equals that of the coherent state, i.e., $N_m(\lambda) = \mu$. Because of the energy increment as a result of photon subtraction, a relatively lower value of λ is required for fulfilling the singularity condition, which is evident from Fig. 1(b). Incidentally, we have observed that far from the optimal working point $\pi/2$, PASSV can still provide some advantage, even under energy-balancing conditions, as shown in Fig. 3, without surpassing the sensitivity obtained by SSV in the optimal point. Typically, this happens from a value of λ in a middle range (namely, $\mu/100 < \lambda < \mu/10$).

Next, we will see the performance of PASSV in the quantum Fisher information perspective.

B. Quantum Fisher information

Quantum Fisher information (QFI) F_Q can be used to identify the lower uncertainty attainable in a parameter estimation problem according to the expression

$$U(\phi) \geq \frac{1}{\sqrt{F_Q(\phi)}}. \quad (4)$$

For the class of pure states [48], QFI takes the following compact form:

$$F_Q(\phi) = 4\langle(\Delta\hat{H})^2\rangle_{|\Psi\rangle_{1,2}}, \quad (5)$$

where \hat{H} is the generator of the unitary transformation associated with the parameter ϕ , i.e., $\hat{U}(\phi) = e^{i\hat{H}\phi}$, and $|\Psi\rangle_{1,2}$ are the input states injected into the interferometer. In the case of the MZI in Fig. 2, the generator is the photon-number operator $\hat{n}_3 = \hat{a}_3^\dagger \hat{a}_3$, where $\hat{a}_3 = (\hat{a}_1 + \hat{a}_2)/\sqrt{2}$. Per Eq. (5), we shall evaluate QFI by considering PASSVs and coherent states injected into the interferometer. The complete expressions for the QFI are cumbersome: graphical representation can help

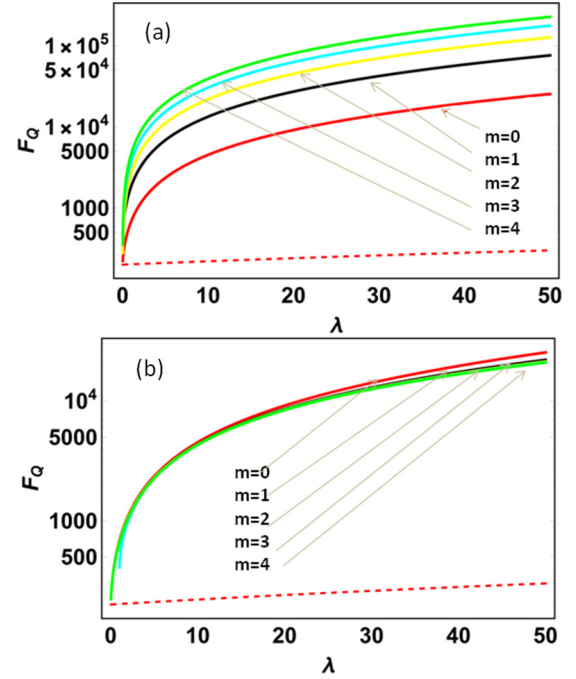


FIG. 4. Quantum Fisher information versus the mean number of photons λ with $\mu = 100$ for different numbers of photon subtraction m : $m = 0$ (solid red line), $m = 1$ (solid black line), $m = 2$ (solid yellow line), $m = 3$ (solid cyan line), and $m = 4$ (solid green line). The dotted line represents the classical bound obtained when only a coherent state with the same total energy ($\lambda + \mu$) is in input: (a) without energy balance and (b) the balanced condition.

us to understand its peculiar features. Specifically, Fig. 4(a) shows a general increasing of the QFI for PASSVs with increasing m for both low and high values of λ ; that is, photon subtraction is always advantageous with respect to the best classical strategies (dotted line). This advantage of QFI due to photon subtraction could be due to the increase of the mean number of photons of the input state. Indeed, for the energy-balancing condition, the advantage is completely lost, as is evident from Fig. 4(b) and also from the expression for the QFI in the limit $N_{\text{tot}} \rightarrow \infty$ (at a finite fixed coherent energy) reported here:

$$\begin{aligned} F_{Q(m=0)} &= 2N_{\text{tot}}^2, \\ F_{Q(m=1)} &= \frac{2N_{\text{tot}}^2}{3}, \\ F_{Q(m=2)} &= \frac{2N_{\text{tot}}^2}{5}, \\ F_{Q(m=3)} &= \frac{2N_{\text{tot}}^2}{7}, \\ F_{Q(m=4)} &= \frac{2N_{\text{tot}}^2}{9}. \end{aligned} \quad (6)$$

This confirms that the advantage of the phase parameter estimation in a MZI provided by photon subtraction of the squeezed state is exclusively due to the increasing energy of the field. Using a simple SSV state with the same energy provides similar sensitivity.

III. SPATSV STATES

Starting from the definition of the TSV as the two-mode squeezing operator $\hat{S}_{1,2}(r_{12}e^{i\chi}) = e^{r_{12}e^{i\chi}a_1a_2 - \text{H.c.}}$ applied to the vacuum, the SPATSV can be obtained by the non-Hermitian operation represented as

$$|\Psi_{\text{SPATSV}}^{(m)}(\lambda, \chi)\rangle_{1,2} = \mathbf{N}_m^-(\lambda)(\hat{a}_1)^m(\hat{a}_2)^m\hat{S}_{1,2}|0, 0\rangle_{1,2}, \quad (7)$$

where \mathbf{N}_m^- is the normalization constant, $\lambda = \sinh^2 r_{12}$ is the mean energy (mean photon number) per mode for the TSV, χ is the squeezing angle, and m is the number of subtracted photons. It is possible to express the state in the Fock basis as follows:

$$|\Psi_{\text{SPATSV}}^{(m)}(\lambda, \chi)\rangle_{1,2} = \frac{\mathbf{N}_m^-(\lambda)}{\sqrt{1+\lambda}} \sum_{n=0}^{\infty} \left(\frac{\lambda e^{i\chi}}{1+\lambda}\right)^{\frac{n+m}{2}} \times \frac{(n+m)!}{n!} |n, n\rangle_{1,2}. \quad (8)$$

The normalization constant has the form $\mathbf{N}_m^-(\lambda) = [(m!)^2 \lambda^m P_m(2\lambda + 1)]^{-1/2}$, where P_m is the m th-order Legendre polynomial. Furthermore, using squeezed transformation of mode operators a_j (and the IWOP technique [46]), it is possible to generate the state in Eq. (7) by applying the squeezing operator to an $(m + 1)$ -component superposition of the photon-number states $|\Theta(\lambda, \chi)\rangle_m$ as follows:

$$|\Psi_{\text{SPATSV}}^{(m)}(\lambda, \chi)\rangle_{1,2} = \hat{S}_{1,2}|\Theta^{(m)}(\lambda, \chi)\rangle_{1,2} \quad (9)$$

where

$$|\Theta^{(m)}(\lambda, \chi)\rangle_{1,2} = \sum_{k=0}^m C_k^m(\lambda, \chi) |k, k\rangle_{1,2}, \quad (10)$$

and

$$C_k^m(\lambda, \chi) = e^{i\chi m} \sqrt{\frac{(1+\lambda)^m}{P_m(2\lambda+1)}} e^{i\chi k} \binom{m}{k} \left(\sqrt{\frac{\lambda}{\lambda+1}}\right)^k, \quad (11)$$

with $\sum_k |C_k^m(\lambda, \chi)|^2 = 1$. Interestingly, $|\Theta^{(m)}(\lambda, \chi)\rangle_{1,2}$ is similar to a truncated TSV up to the components with $k \leq m$. As can be seen by a careful inspection of $C_k^m(\lambda, \chi)$, they differ only by a binomial coefficient and a normalization factor. For $m = 0$ the state $|\Psi_{\text{SPATSV}}^{(0)}(\lambda, \chi)\rangle_{1,2}$ coincides obviously with TSV. For $m = 1$, namely, one-photon subtraction, the corresponding normalized two-component photon-number superposition state is

$$|\Theta^{(1)}(\lambda, \chi)\rangle_{1,2} = \frac{1}{\sqrt{2\lambda+1}} (\sqrt{1+\lambda}|0, 0\rangle + e^{i\chi}\sqrt{\lambda}|1, 1\rangle). \quad (12)$$

This superposition state is entangled for nonzero values of λ and resembles to the state [41], and for $\lambda \gg 1$ it becomes asymptotically a maximally entangled state. In general, Eqs. (9), (10), and (11) suggest that a SPATSV state can be generated by seeding the input modes of a nonlinear two-mode-squeezing interaction by an opportune superposition state in the photon-number basis [see Fig. 5(b)]. This represents an alternative way to generate the photon-subtracted states in contrast to the common approach depicted in Fig. 5(a), consisting of a postselection of the

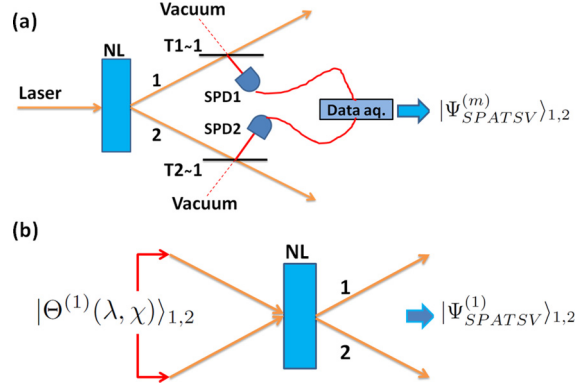


FIG. 5. Generation scheme for the SPATSV state with symmetric photon subtraction of one photon $m = 1$: (a) Probabilistic process by two beam splitters of high transmittance $T_1 = T_2 \approx 1$ placed in two arms of the PDC source. Simultaneous clicks on the two single-photon detectors confirm the generation of SPATSV. (b) An alternative approach to the generation of SPATSV consists of injecting the seeding state of the general form in Eq. (10) into the nonlinear crystal (NL), in particular the one reported in Eq. (12) for the case $m = 1$.

state, conditioned on double-click events at the detectors placed in the two arms, experimentally realized through an unbalanced BS.

A. Squeezing properties and photon statistics of the SPATSV state

Analogous to what has already been discussed in Sec. II for single-mode states [43,44], two-mode superposition states $|\Theta^{(m)}(\lambda, \chi)\rangle_{1,2}$ are also squeezed in the quadrature difference even though they do not minimize the uncertainty principle. The maximum squeezing is reached for

$$\hat{X}_\chi^- = \hat{X}_{1,\chi} - \hat{X}_{2,\chi}, \quad (13)$$

where $\hat{X}_{j,\chi} = (\hat{a}_j e^{-i\chi} + \hat{a}_j^\dagger e^{i\chi})/\sqrt{2}$ is the quadrature of the j th individual input mode. This is reported in Fig. 6(a). Note that for $m \geq 1$ nonclassical correlations are always present, becoming stronger with increasing m in the region of small λ . When $m \geq 2$, the squeezing level overcomes the TSV limit (dotted purple line). The quadrature noise behavior of the seeding state has a direct effect on the squeezing properties of the SPATSV, as shown in Fig. 6(b), basically leading to a further noise reduction, especially for $\lambda < 1$ with respect to the TSV state. This effect is not trivially related to an energy shift, and it can be beneficial when using the SPATSV state for specific interferometric schemes, as discussed in Sec. III B. Aside from quadrature squeezing, other statistical properties of the field can be improved in terms of noise reduction and turned to the nonclassical regime by the photon-subtraction operation. Indeed, postselecting the components of the state with at least one photon induces a shrinking of the photon-number distribution because of the elimination of the vacuum component. On the one hand, it leads to a shift to a higher value of the mean photon number per mode $\mathcal{L}_m(\lambda) \geq \lambda$, as shown in Fig. 7. On the other hand, it induces a sub-shot-noise behavior in each of the two modes.

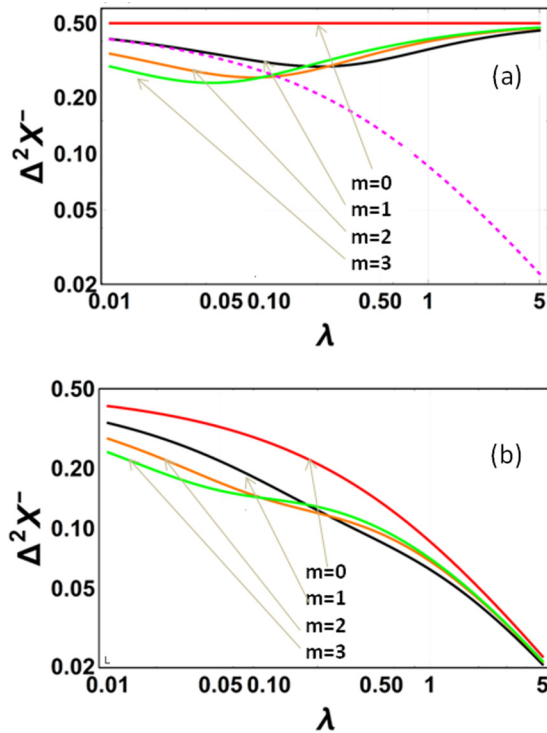


FIG. 6. Nonclassical amplitude quadrature correlation (0.5 is the classical bound) versus λ for different number of photon subtraction m : $m = 0$ (solid red line), $m = 1$ (solid black line), $m = 2$ (solid orange line), and $m = 3$ (solid green line). The plots refer to a) for superposition state $|\Theta^{(m)}(\lambda, \chi)\rangle_{1,2}$, except the dotted curve which corresponds to TSV and b) the photon subtracted SPASTV state.

Nonclassicality in the photon-number statistics is usually described by Mandel’s Q parameter [47]:

$$Q = \frac{\text{Var}(\hat{N}) - \langle \hat{N} \rangle}{\langle \hat{N} \rangle}, \quad (14)$$

where $\hat{N} = \hat{a}^\dagger \hat{a}$ is the photon-number operator. For classical light Mandel’s parameter is bounded by $Q \geq 0$. It is worth noting that the individual modes of TSV have thermal statistics, but once we apply the subtraction operation with $m > 1$, they become nonclassical for low mean photon numbers, which is evident from the negative value of Mandel’s parameter reported in Fig. 8. This nonclassical behavior induced by photon subtraction is clearly not related to an energy shift of the single mode (which would conserve thermal statistics); rather, it is a more fundamental uncertainty reduction of the photon-number distribution.

B. Correlated-phase estimation with SPASTV states

The interferometry system we consider in this section is presented in Fig. 9. It is composed of two linear interferometers, for instance, a pair of MZIs whose photocurrents at the readout ports are jointly measured. This is an elegant and powerful scheme in the detection of extremely faint phase signals whose magnitude can be much smaller than other sources of noise, including the shot noise. The advantage of this scheme comes from the fact that the same signal shared by the two interferometers, even if hidden in the

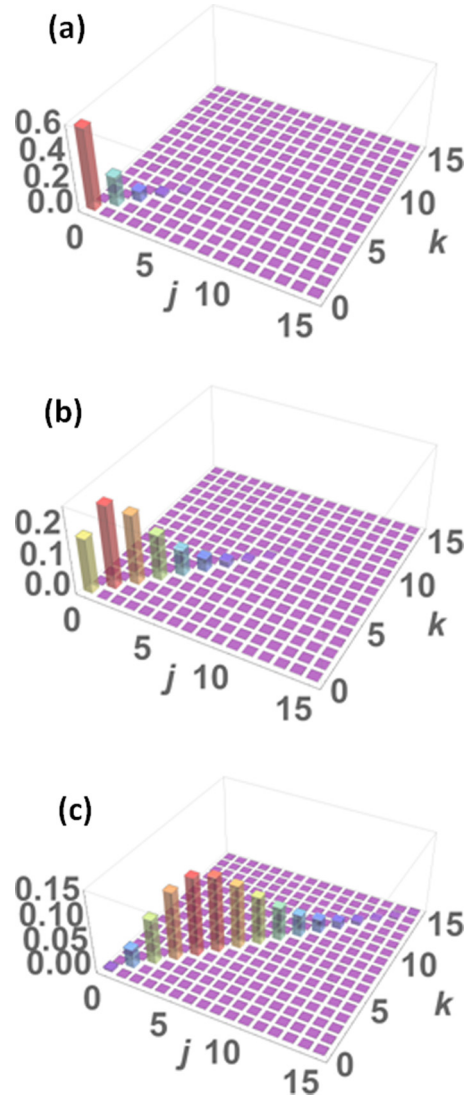


FIG. 7. Three-dimensional plots showing the joint photon-number distribution in the SPASTV state. j and k are the photon numbers in modes 1 and 2, respectively. The parameter values chosen are $\lambda = 0.6$ and (a) $m = 0$, (b) $m = 1$, and (c) $m = 3$.

noise in the single device, can be found by correlating their outputs. This strategy has already been considered in several highly demanding applications, in general related to the research on stochastic fundamental backgrounds, such as the gravitational-wave background [50–53] and quantum gravity effects at the Planck scale [54,55].

The advantage of using the quantum state of light in such a configuration was analyzed in Refs. [56,57]. It was shown that injection of the quantum state of light in the classically unused input ports (labeled 1 and 2 in Fig. 9), either as two independent squeezed states or as a TSV, allows us to achieve better sensitivities. In the case of a TSV, for specific working conditions, i.e., very close to the dark fringes and for high quantum efficiency, the quantum advantage is dramatic even with respect to the double squeezing. Here our purpose is to investigate if and to what extent a photon-subtracted TSV allows us to obtain better performance in light of their improved nonclassical properties discussed in Sec. III A.

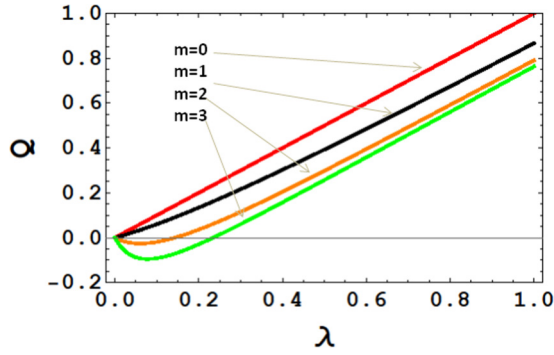


FIG. 8. Mandel's Q of the SPATSV state as a function of the mean photon number per mode λ for different numbers of photon subtraction m : $m = 0$ (solid red line), $m = 1$ (solid black line), $m = 2$ (solid orange line), and $m = 3$ (solid green line). Here, we have chosen $\eta = 0.98$.

1. Noise-reduction factor at the readout ports

Let us start by considering the correlation properties of the readout signals at the output ports (labeled 5 and 7 in Fig. 9). In particular we are interested in photocurrent subtraction, proportional to the photon-number difference $\hat{N}_5 - \hat{N}_7$.

Here we consider the noise-reduction factor, a standard measure of nonclassical correlation for a bipartite state defined as [58]

$$\sigma = \frac{\langle \Delta^2(\hat{N}_5 - \hat{N}_7) \rangle}{\langle \hat{N}_5 \rangle + \langle \hat{N}_7 \rangle}. \tag{15}$$

The numerator is the variance of the photon-number difference, and the denominator represents the standard quantum limit. Thus, $\sigma < 1$ indicates nonclassical correlation. It is convenient to introduce the factor $\tau = \cos^2(\phi/2)$, representing the fraction of the power at the input port 1 (2), transmitted to the readout port 5 (7). Consequently, $1 - \tau$ is the equivalent loss experienced by the quantum modes due to the interference fringe position and, at the same time, the fraction of coherent power injected at port 3 (4) and transmitted to the output port 5 (7). The NRF has been evaluated analytically

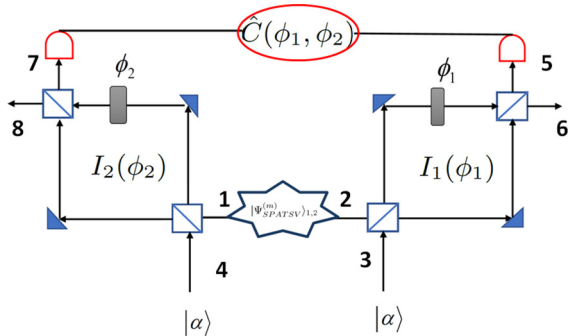


FIG. 9. Correlated interferometric scheme: The modes of the bipartite input state $|\Psi_{\text{SPATSV}}^{(m)}(\lambda, \chi)\rangle_{1,2}$ are mixed with two identical coherent states $|\alpha\rangle = |\mu e^{i\psi}\rangle$ in two interferometers $I_1(\phi_1)$ and $I_2(\phi_2)$. A joint detection is performed and the observable $\hat{C}(\phi_1, \phi_2)$ is measured. The losses are accounted by considering two identical detectors in both channels with the same quantum efficiency, i.e., $\eta_5 = \eta_7 = \eta$.

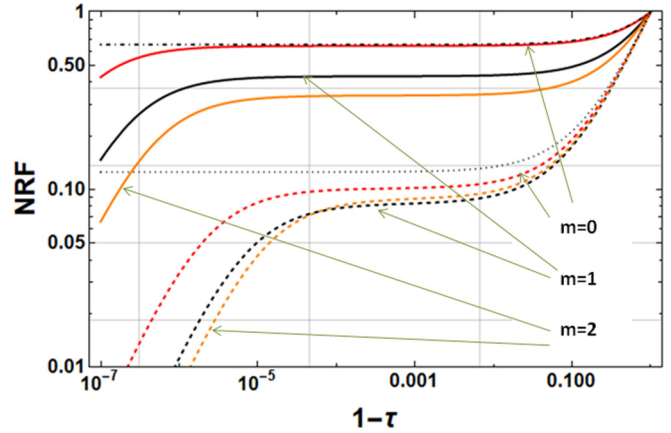


FIG. 10. Noise-reduction factor at output ports 5 and 7 of the interferometers as a function of the transmittance parameter $1 - \tau = \sin^2 \phi/2$ for different numbers of photon subtraction m : $m = 0$ (red line), $m = 1$ (black line), and $m = 2$ (orange line). Solid thick lines are for $\lambda = 0.05$, and dashed lines stand for $\lambda = 2$. Asymptotic limits for $\lambda \gg 1$ and for $\lambda \ll 1$ ($m = 0$) are the dotted and the dot-dashed lines, respectively. The other parameters are $\eta = 1$, $\psi = \pi/2$, $\mu = 10^6$.

and is reported in Fig. 10 as a function of $1 - \tau$. In order to analyze its behavior let us distinguish between two regimes. When the output signal is dominated by a photon coming from the coherent beam, i.e., $\mathcal{L}_m(\lambda)\tau \ll \mu(1 - \tau)$ [we recall that $\mathcal{L}_m(\lambda)$ is the SPATSV mean photon number], each interferometer acts similarly to a homodyne detector. This represents the typical working condition since, usually, the coherent beam is several orders of magnitude brighter than the quantum light and corresponds roughly to the region $1 - \tau > 10^{-4}$ in Fig. 10. In this case, the difference in the photon number at output ports 5 and 7 becomes approximately proportional to the difference between the quadrature of the input modes at ports 1 and 2:

$$\hat{N}_5 - \hat{N}_7 \propto \sqrt{\frac{\mu}{2}} \sin(\phi) \hat{X}_{\psi+\pi/2}^- \tag{16}$$

where ψ can be chosen to match the angle of the squeezed quadrature difference in Eq. (13), in particular $\psi = \chi - \pi/2$. Therefore, the nonclassical correlation of the input state reported in Fig. 6(b) immediately traduces the nonclassical properties of the NRF. In particular, for $\lambda \gg 1$ the NRF is well approximated by $\sigma_m(\lambda) \approx 1 - \tau + \tau/(4\lambda)$ (the dashed line in Fig. 10) for all numbers of subtracted photons m (for $1 - \tau > 10^{-4}$). Also, for $\lambda \ll 1$, i.e., when the quadrature squeezing of the SPATSV states increases with the number of subtracted photons, the NRF follows the same behavior, demonstrating the advantage of using photon-subtracted states, as clearly shown in Fig. 10. Analytically, it can be found that in this asymptotic limit of $\lambda \ll 1$ the expression of the NRF at different orders of photon subtraction can be approximated as

$$\sigma_{m=0} \approx 1 - 2\tau(\sqrt{\lambda} - \lambda), \tag{17}$$

$$\sigma_{m=1} \approx 1 - 4\tau(\sqrt{\lambda} - 2\lambda), \tag{18}$$

$$\sigma_{m=2} \approx 1 - 6\tau(\sqrt{\lambda} - 3\lambda), \tag{19}$$

where the first of these equations is reported in Fig. 10 as the dot-dashed line.

In the opposite scenario, when the coherent beam does not contribute significantly to the outputs and the two interferometers, i.e., $\mathcal{L}_m\tau \gg \mu(1-\tau)$, the interferometers can be seen as attenuators with transmission τ of the input state. The photon-number entanglement between the two modes of the SPATSV input state is then preserved at the output ports for $\tau \sim 1$. Indeed, in the ideal case of $\phi = 0$ ($\tau = 1$) and unit detection efficiency, the photon-number correlation at the output ports 5 and 7 is perfect, independent of the energy λ of the input quantum state. This explains the sudden dropping down of the NRF observed in Fig. 10 for $1-\tau < 10^{-4}$. However, the condition $\mathcal{L}_m\tau \gg \mu(1-\tau)$ is reached for a smaller value of τ (higher value of ϕ) when the input energy $\mathcal{L}_m(\lambda)$ is larger. So, recalling that $\mathcal{L}_{m+1}(\lambda) > \mathcal{L}_m(\lambda)$, if the energy λ of the TSV before the photon subtraction is fixed, subtracting more photons makes it easier to reach the region in which entanglement determines a dramatic reduction of the uncertainty. In the next section we shall show that the characteristics of the NRF are strictly related to the sensitivity of the double interferometric setup.

2. Phase correlation estimation

In the setup of Fig. 9, rather than the magnitude of phase noise in the single MZI, the quantity being estimated is the covariance between the phase fluctuations in two interferometers. This estimate can somehow be related to a joint measurement of the readout signals N_5 and N_7 . In the limit of a faint signal, any joint observable $\hat{C}(\phi_1, \phi_2) = \hat{C}(N_5(\phi_1), N_7(\phi_2))$ with a local non-null double partial derivative $\partial_{\phi_1, \phi_2}^2 \hat{C}(\phi_1, \phi_2)$ can be exploited for a phase-noise covariance estimation [57]. Here the goal is to investigate whether SPATSV can lead to some sensitivity advantage with respect to the TSV state in that scheme. The uncertainty in the phase covariance measurement is [56]

$$\mathcal{U} = \frac{\sqrt{2 \text{Var}[\hat{C}(\phi_1, \phi_2)]}}{|\partial_{\phi_1, \phi_2}^2 \hat{C}(\phi_1, \phi_2)|}. \quad (20)$$

A good choice for the joint measurement operator is $\hat{C}(\phi_1, \phi_2) = [N_5(\phi_1) - N_7(\phi_2)]^2 = N_5^2 + N_7^2 - 2N_5N_7$. On the one hand, according to the results for the NRF discussed in Sec. III B 1, it has a fluctuation below the classical limit. On the other, it satisfies the condition $\partial_{\phi_1, \phi_2}^2 \hat{C}(\phi_1, \phi_2) \neq 0$. The classical bound, obtained with coherent states at ports 3 and 4 and vacuum at ports 1 and 2, is given by $\mathcal{U}_{cl} = \sqrt{2}(\eta\mu \cos^2[\phi/2])^{-1}$ [57], where we have introduced the detection efficiency η , assumed to be equal in the two channels. Hereinafter, we present the uncertainties U_m for the m th SPATSV state, as normalized to the coherent classical limit, namely, $U_m = \mathcal{U}_m/\mathcal{U}_{cl}$.

Analytical results of uncertainties as a function of the working central phase $\phi_1 = \phi_2 = \phi$ are plotted in Fig. 11. Similar to the case of the NRF analyzed in the previous section, one can distinguish two different regions: one lying roughly in the range $10^{-5} < \phi < \pi$ (shown up to $\phi \approx 10^{-3}$ in Fig. 11) and the other for a smaller value of the phase, $\phi \ll 10^{-6}$, separated by a short transient. The range $10^{-5} < \phi < \pi$ corresponds to the situation in which the mean number

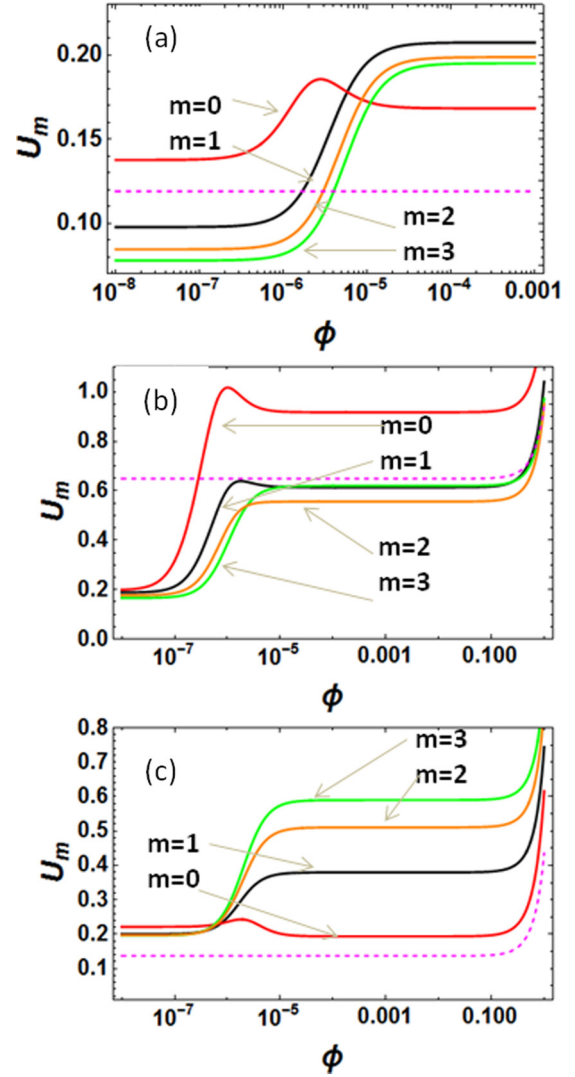


FIG. 11. Normalized uncertainty as a function of ϕ with $\mu = 10^{12}$ for different numbers of photon subtraction m : $m = 0$ (solid red line), $m = 1$ (solid black line), $m = 2$ (solid orange line), and $m = 3$ (solid green line). The dashed purple line represents two independent squeezed states: (a) $\lambda = 2$, $\eta = 0.98$ and (b) $\lambda = 0.05$, $\eta = 0.98$. (c) Energy-balancing scenario for $\lambda = 2$, $\eta = 0.96$.

of coherent photons at the readout ports is much larger than the transmitted SPATSV photons [i.e., $\mathcal{L}_m(\lambda)\tau \ll \mu(1-\tau)$]. In this case, the quadrature nonclassical correlation of the input modes is responsible for the readout signal correlation. To provide compact expressions we have reported analytical results in relevant regimes. In the limit of high coherent power, $\mu \gg 1$, and low squeezing, $\lambda \ll 1$, one gets

$$U_{m=0} \approx \sqrt{2}[1 - \tau\eta(2\sqrt{\lambda} - 2\lambda)], \quad (21)$$

$$U_{m=1} \approx \sqrt{2}[1 - \tau\eta(4\sqrt{\lambda} + \frac{1}{2}\lambda(3\eta\tau - 16))], \quad (22)$$

$$U_{m=2} \approx \sqrt{2}[1 - \tau\eta(6\sqrt{\lambda} + \frac{9}{2}\lambda(\eta\tau - 4))], \quad (23)$$

$$U_{m=3} \approx \sqrt{2}[1 - \tau\eta(8\sqrt{\lambda} + \lambda(9\eta\tau - 32))]. \quad (24)$$

Note that these expressions follow the NRF behavior reported in Eqs. (17), (18), and (19) up to the terms in $\sqrt{\lambda}$. It turns out

that asymptotically, for $\lambda \ll 1$, there is an advantage which increases with the number of subtracted photons m . However, when the asymptotic condition is not fully fulfilled, i.e., for finite values of the SPATSV energy $\mathcal{L}_m(\lambda)$, higher values of m do not always correspond to lower uncertainties, as reported in Fig. 11(b) in the range $\phi > 10^{-5}$, e.g., for $\lambda = 0.05$. Moreover, Eqs. (21)–(24) show that the detection efficiency η plays the same role as the interferometer transmission τ and both of them should be high enough to ensure a significant quantum advantage.

In the case of strong squeezing, $\mu \gg \lambda \gg 1$, provided the condition $\mathcal{L}_m(\lambda)\tau \ll \mu(1 - \tau)$ is still fulfilled, it turns out that the U_m 's respective expressions for different values of m do not differ much; in fact, we have

$$U_{m=0,1,2,3} \approx \sqrt{2} \left(1 - \tau\eta - \frac{\tau\eta}{4\lambda} \right) \quad (25)$$

Also in this case, some deviation from the asymptotic behavior can emerge when finite values of the parameters are considered. For instance, the case $\lambda = 2$ is reported in Fig. 11(a).

The opposite situation, when the number of SPATSV photons is dominant with respect to the coherent ones at readout ports 5 and 7 [$\mathcal{L}_m\tau \gg \mu(1 - \tau)$], corresponds in Fig. 11 to the range $\phi \ll 10^{-6}$. Perfect photon-number correlation of the SPATSV entangled state at input ports 2 and 3 is preserved between N_5 and N_7 . For $\mu \gg 1$ (and $\phi \rightarrow 0$) we obtain the following asymptotic behavior:

$$U_{m=0,1,2,3} \approx \sqrt{2} \sqrt{(1 - \eta)/\eta} \quad \lambda \ll 1, \quad (26)$$

$$U_{m=0} \approx 2\sqrt{5}(1 - \eta) \quad \lambda \gg 1,$$

$$U_{m=1} \approx 2\sqrt{3}(1 - \eta),$$

$$U_{m=2} \approx 2\sqrt{13/5}(1 - \eta),$$

$$U_{m=3} \approx 2\sqrt{17/7}(1 - \eta). \quad (27)$$

Equations (26) and (27) show that in this regime of perfect photon-number correlations the uncertainty reduction is mainly limited by the detection efficiency. This means that there always exists a value of the efficiency high enough to make this regime more advantageous with respect to the one exploiting the quadrature correlation. For example, in Fig. 11, $\eta = 0.98$ guarantees a stronger advantage for $\phi \ll 10^{-6}$. From Eq. (27) it is evident that only for $\lambda \gg 1$, the uncertainty reduction depend on the number of subtracted photons m . In addition, photon subtraction brings a further improvement: the increasing of the energy \mathcal{L}_m with m (at fixed λ) extends the range of validity of the photon-number-correlation advantage, $\mathcal{L}_m\tau \gg \mu(1 - \tau)$, towards higher values of ϕ , as shown in Fig. 11.

It is relevant to understand whether the uncertainty reduction observed for SPATSV states can be explained only in terms of the mean energy increasing due to the photon-subtraction operation or whether the advantage comes from other properties of these states. Also in this case, we consider the energy-balancing approach in Sec. II A, where the energies of two-mode photon-subtracted states ($m = 0, 1, 2, 3$) are made equivalent to the energy of TSV, and we observe that the uncertainty reduction advantage in the high-detection-efficiency cases [Figs. 11(a) and 11(b)] almost disappears

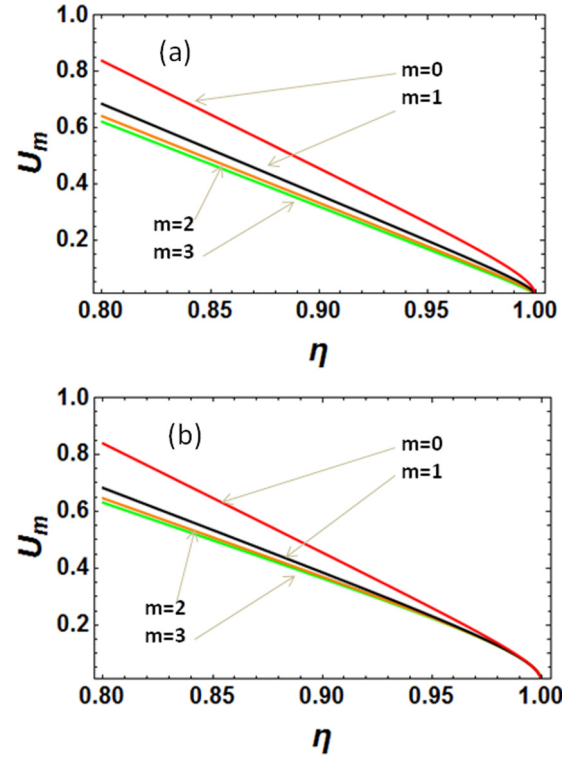


FIG. 12. Normalized uncertainty versus the detection efficiency η with $\mu = 10^{12}$, $\lambda = 2$, and $\phi = 10^{-8}$ for different numbers of photon subtraction m : $m = 0$ (solid red line), $m = 1$ (solid black line), $m = 2$ (solid orange line), and $m = 3$ (solid green line), (a) without energy balancing and (b) for the balanced-energy condition.

[see Fig. 11(c)]. However, in the case of a realistic value of the detection efficiency and optical losses, we observe that the improvement of the uncertainty reduction is still present (Fig. 12). For instance, in this scenario SPATSV with $m = 3$ presents around 26% of an uncertainty reduction advantage compared to TSV at a detection efficiency of 0.8. Thus, the uncertainty reduction obtained with SPATSV states is, in general, due not only to the energy shifts but also to the enhancement in mode correlation and statistics.

IV. SUMMARY AND CONCLUSIONS

We have studied in detail multiphoton-subtracted one- and two-mode squeezed vacuum state, in relation to phase estimation in both single- and correlated-phase interferometry. The squeezing of the single-mode PASSV state does not necessarily improve with the number of subtracted photons. In the case of an odd number for photon subtraction, it is definitely worse than SSV, while for even photon subtraction, it is better than the SSV only for a relatively small brightness. The phase estimation uncertainty in a single interferometer reflects this behavior, as expected. Moreover, by comparing the phase sensitivity after readjusting the energy of the PASSVs to match that of the SSV, the advantage of the photon subtraction disappears, at least at the optimal working point of $\phi = \pi/2$. For other values of the central operating phase we have a different behavior, and in some cases, as shown in Fig. 3,

the advantage of photon subtraction is preserved even when energies are balanced.

In terms of QFI, we have found improvements in the number of subtracted photons, but for the energy-balancing condition this advantage disappears. However, the Heisenberg limit can be reached for an asymptotically large number of photons in a lossless interferometer.

We also investigated SPATSV for correlated interferometry [56,57]. Usually, such SPATSV states are generated by probabilistic events with a low success rate. We showed analytically how symmetric photon subtraction from a two-mode squeezed vacuum is equivalent to the squeezing of a finite-component superposition state, suggesting an alternative way to generate SPATSV states. We found that these SPATSV states always show quadrature squeezing and their strength increases with symmetrical photon number subtraction for a small energy of the state. Various statistical properties, including photon-number distribution, Mandel's Q function, and the noise-reduction factor, show a higher nonclassical signature of SPATSV with respect to TSV, suggesting its potential advan-

tages in a correlated phase estimation. In fact, concerning the phase correlation measurement among two interferometers, we observed that SPATSVs are able to achieve a smaller uncertainty than TSVs for an operation point close to the dark fringe ($\phi \approx 0$). In the low-loss scenario, SPATSVs apparently provide a substantial advantage in uncertainty reduction with respect to TSV states, but this is essentially explained by the energy increase of the states due to the photon subtraction. In fact, renormalizing the energies of the SPATSV to that of the initial TSV state, the uncertainty reduction is lost. However, SPATSVs retain an advantage of about 30% with respect to TSVs in the high-loss scenario, and this can be attributed to their improved statistical properties.

ACKNOWLEDGMENTS

This work has been sponsored by the EU via "Quantum readout techniques and technologies" (QUARTET, Grant Agreement No. 862644) and by the EMPIR Participating States in the context of the project 17FUN01 BeCOME.

-
- [1] M. G. Genoni and M. G. A. Paris, Quantifying non-Gaussianity for quantum information, *Phys. Rev. A* **82**, 052341 (2010).
 - [2] S. Olivares, M. G. A. Paris, and R. Bonifacio, Teleportation improvement by inconclusive photon subtraction, *Phys. Rev. A* **67**, 032314 (2003).
 - [3] T. Opatrny, G. Kurizki, and D.-G. Welsch, Improvement on teleportation of continuous variables by photon subtraction via conditional measurement, *Phys. Rev. A* **61**, 032302 (2000).
 - [4] P. T. Cochrane, T. C. Ralph, and G. J. Milburn, Teleportation improvement by conditional measurements on the two-mode squeezed vacuum, *Phys. Rev. A* **65**, 062306 (2002).
 - [5] F. Dell'Anno, S. De Siena, and F. Illuminati, Realistic continuous-variable quantum teleportation with non-Gaussian resources, *Phys. Rev. A* **81**, 012333 (2010).
 - [6] L. F. M. Borelli, L. S. Aguiar, J. A. Roversi, and A. Vidiella-Barranco, Quantum key distribution using Continuous-variable non-Gaussian States, *Quantum Inf. Process.* **15**, 893 (2016).
 - [7] Q. Liao, Y. Guo, D. Huang, P. Huang, and G. Zeng, Long-distance continuous-variable quantum key distribution using non-Gaussian state-discrimination detection, *New J. Phys.* **20**, 023015 (2018).
 - [8] N. J. Cerf, O. Kruger, P. Navez, R. F. Werner, and M. M. Wolf, Non-Gaussian Cloning of Quantum Coherent States Is Optimal, *Phys. Rev. Lett.* **95**, 070501 (2005).
 - [9] J. Eisert, S. Scheel, and M. B. Plenio, Distilling Gaussian States with Gaussian Operations is Impossible, *Phys. Rev. Lett.* **89**, 137903 (2002).
 - [10] G. Giedke and J. I. Cirac, The characterization of Gaussian operations and distillation of Gaussian states, *Phys. A* **66**, 032316 (2002).
 - [11] J. Fiurasek, Gaussian transformations and distillation of entangled Gaussian states, *Phys. Lett.* **89**, 137904 (2002).
 - [12] J. Niset, J. Fiurasek, and N. J. Cerf, No-go theorem for gaussian quantum error correction, *Phys. Lett.* **102**, 120501 (2009).
 - [13] F. Ferreyrol, M. Barbieri, R. Blandino, S. Fossier, R. Tualle-Brouri, and P. Grangier, Implementation of a nondeterministic optical noiseless amplifier, *Phys. Lett.* **104**, 123603 (2010).
 - [14] G. Y. Xiang, T. C. Ralph, A. P. Lund, N. Walk, and G. J. Pryde, Heralded noiseless linear amplification and distillation of entanglement, *Nat. Photonics* **4**, 316 (2010).
 - [15] K. Banaszek and K. Wódkiewicz, Nonlocality of the Einstein-Podolsky-Rosen State in the Wigner Representation, *Phys. Rev. A* **58**, 4345 (1998).
 - [16] H. Nha and H. J. Carmichael, Proposed Test of Quantum Nonlocality for Continuous Variables, *Phys. Rev. Lett.* **93**, 020401 (2004).
 - [17] R. Takagi and Q. Zhuang, Convex resource theory of non-Gaussianity, *Phys. Rev. A* **97**, 062337 (2018).
 - [18] F. Albarelli, M. G. Genoni, M. G. A. Paris, and A. Ferraro, Resource theory of quantum non-Gaussianity and wigner negativity, *Phys. Rev. A* **98**, 052350 (2018).
 - [19] M. G. Genoni, C. Invernizzi, and M. G. A. Paris, Enhancement of parameter estimation by Kerr interaction, *Phys. Rev. A* **80**, 033842 (2009).
 - [20] R. Carranza and C. C. Gerry, Photon-subtracted two-mode squeezed vacuum states and applications to quantum-optical interferometry, *J. Opt. Soc. Am. B* **29**, 2581 (2012).
 - [21] M. S. Kim, Recent developments in photon-level operations on traveling light fields, *J. Phys. B* **41**, 133001 (2008).
 - [22] M. Kim, The quantum mechanics of photon addition and subtraction, SPIE Newsroom, <https://doi.org/10.1117/2.1200811.1369> (2008).
 - [23] V. Parigi, A. Zavatta, M. S. Kim, and M. Bellini, Probing quantum commutation rules by addition and subtraction of single photons to/from a light field, *Science* **317**, 1890 (2007).
 - [24] G. S. Agarwal and K. Tara, Nonclassical properties of states generated by the excitations on a coherent state, *Phys. Rev. A* **43**, 492 (1991).
 - [25] A. Zavatta, S. Viciani, and M. Bellini, Quantum-to-classical transition with single-photon-added coherent states of light, *Science* **306**, 660 (2004).

- [26] A. Zavatta, V. Parigi, and M. Bellini, Experimental nonclassicality of single-photon-added thermal light states, *Phys. Rev. A* **75**, 052106 (2007).
- [27] C. Navarrete-Benlloch, R. García-Patrón, J. H. Shapiro, and N. J. Cerf, Enhancing quantum entanglement by photon addition and subtraction, *Phys. Rev. A* **86**, 012328 (2012).
- [28] T. J. Bartley, P. J. D. Crowley, A. Datta, J. Nunn, L. Zhang, and I. A. Walmsley, Strategies for enhancing quantum entanglement by local photon subtraction, *Phys. Rev. A* **87**, 022313 (2013).
- [29] A. Ourjoumtsev, A. Dantan, R. Tualle-Brouri, and P. Grangier, Increasing Entanglement between Gaussian States by Coherent Photon Subtraction, *Phys. Rev. Lett.* **98**, 030502 (2007).
- [30] T. S. Iskhakov, V. C. Usenko, R. Filip, M. V. Chekhova, and G. Leuchs, Low-noise macroscopic twin beams, *Phys. Rev. A* **93**, 043849 (2016).
- [31] S. L. Zhang, J. S. Guo, W. S. Bao, J. H. Shi, C. H. Jin, X. B. Zou, and G. C. Guo, Quantum illumination with photon subtracted continuous variable entanglement, *Phys. Rev. A* **89**, 062309 (2014).
- [32] S. Lloyd, Enhanced sensitivity of photo detection via quantum illumination, *Science* **321**, 1463 (2008).
- [33] E. D. Lopaeva, I. R. Berchera, I. P. Degiovanni, S. Olivares, G. Brida, and M. Genovese, Experimental Realization of Quantum Illumination, *Phys. Rev. Lett.* **110**, 153603 (2013).
- [34] R. Birrittella and C. C. Gerry, Quantum optical interferometry via the mixing of coherent and photon-subtracted squeezed vacuum states of light, *J. Opt. Soc. Am. B* **31**, 586 (2014).
- [35] Y. Ouyang, S. Wang, and L. Zhang, Quantum optical interferometry via the photon added two-mode squeezed vacuum states, *J. Opt. Soc. Am. B* **33**, 1373 (2016).
- [36] C. M. Caves, Quantum-mechanical noise in an interferometer, *Phys. Rev. D* **23**, 1693 (1981).
- [37] M. Tse, H. Yu, N. Kijbunchoo, A. Fernandez-Galiana, P. Dupej, L. Barsotti, C. D. Blair, D. D. Brown, S. E. Dwyer, A. Effler *et al.*, Increasing the Astrophysical Reach of the Advanced Virgo Detector via the Application of Squeezed Vacuum States of Light, *Phys. Rev. Lett.* **123**, 231107 (2019).
- [38] F. Acernese, M. Agathos, L. Aiello, A. Allocca, A. Amato, S. Ansoldi, S. Antier, M. Arène, N. Arnaud, S. Ascenzi *et al.*, Increasing the Astrophysical Reach of the Advanced Virgo Detector via the Application of Squeezed Vacuum States of Light, *Phys. Rev. Lett.* **123**, 231108 (2019).
- [39] R. Demkowicz-Dobrzański, K. Banaszek, and R. Schnabel, Fundamental quantum interferometry bound for the squeezed-light-enhanced gravitational wave detector GEO 600, *Phys. Rev. A* **88**, 041802(R) (2013).
- [40] S. Olivares, M. Popovic, and M. G. A. Paris, Phase estimation with squeezed single photons, *Quantum Meas. Quantum Metrol.* **3**, 38 (2016).
- [41] F. Dell'Anno, S. De Siena, L. Albano, and F. Illuminati, Continuous-variable quantum teleportation with non-Gaussian resources, *Phys. Rev. A* **76**, 022301 (2007).
- [42] P. Marek, J. Provatnizic, and R. Filip, Loop-based subtraction of a single photon from a traveling beam of light, *Opt. Express* **26**, 29837 (2018).
- [43] K. Wodkiewicz, P. L. Knight, S. J. Buckle, and S. M. Barnett, Squeezing and superposition states, *Phys. Rev. A* **35**, 2567 (1987).
- [44] P. Figurny, A. Orłowski, and K. Wodkiewicz, Squeezed fluctuations of truncated photon operators, *Phys. Rev. A* **47**, 5151 (1993).
- [45] K. Thapliyal, N. Samantaray, J. Banerji, and A. Pathak, Comparison of lower- and higher-order nonclassicality in photon added and subtracted squeezed coherent states, *Phys. Lett. A* **381**, 3178 (2017).
- [46] H. Y. Fan, Operator ordering in quantum optics theory and the development of Dirac's symbolic method, *J. Opt. B* **5**, R147 (2003).
- [47] L. Mandel and E. Wolf, *Optical Coherence and Quantum Optics* (Cambridge University Press, Cambridge, 1995).
- [48] R. Demkowicz-Dobrzański, M. Jarzyna, and J. Kolodnyński, Quantum limits in optical interferometry, *Prog. Opt.* **60**, 345 (2015).
- [49] L. Pezze and A. Smerzi, Mach-Zehnder Interferometry at the Heisenberg Limit with Coherent and Squeezed-Vacuum Light, *Phys. Rev. Lett.* **100**, 073601 (2008).
- [50] A. Nishizawa, S. Kawamura, T. Akutsu, K. Arai, K. Yamamoto, D. Tatsumi, E. Nishida, M. A. Sakagami, T. Chiba, R. Takahashi, and N. Sugiyama, Optimal location of two laser-interferometric detectors for gravitational wave backgrounds at 100 MHz, *Classical Quantum Gravity* **25**, 225011 (2008).
- [51] J. Abadie, B. P. Abbott, R. Abbott, T. D. Abbott, M. Abernathy, T. Accadia, F. Acernese, C. Adams, R. Adhikari, C. Affeldt *et al.*, Upper limits on a stochastic gravitational-wave background using LIGO and Virgo interferometers at 600–1000 Hz, *Phys. Rev. D* **85**, 122001 (2012).
- [52] A. S. Chou, H. Glass, H. R. Gustafson, C. J. Hogan, B. L. Kamai, O. Kwon, R. Lanza, L. McCuller, S. S. Meyer, J. W. Richardson, C. Stoughton, R. Tomlin, and R. Weiss, Interferometric constraints on quantum geometrical shear noise correlations, *Classical Quantum Gravity* **34**, 165005 (2017).
- [53] A. S. Chou, R. Gustafson, C. J. Hogan, B. Kamai, O. Kwon, R. Lanza, S. L. Larson, L. McCuller, S. S. Meyer, J. Richardson, C. Stoughton, R. Tomlin, and R. Weiss, MHz gravitational wave constraints with decameter Michelson interferometers, *Phys. Rev. D* **95**, 063002 (2017).
- [54] C. J. Hogan, Interferometers as probes of Planckian quantum geometry, *Phys. Rev. D* **85**, 064007 (2012).
- [55] A. S. Chou, R. Gustafson, C. Hogan, B. Kamai, O. Kwon, R. Lanza, L. McCuller, S. S. Meyer, J. Richardson, C. Stoughton, R. Tomlin, S. Waldman, and R. Weiss, First Measurements of High Frequency Cross-Spectra from a Pair of Large Michelson Interferometers, *Phys. Rev. Lett.* **117**, 111102 (2016).
- [56] I. R. Berchera, I. P. Degiovanni, S. Olivares, and M. Genovese, Quantum Light in Coupled Interferometers for Quantum Gravity Tests, *Phys. Rev. Lett.* **110**, 213601 (2013).
- [57] I. Ruo-Berchera, I. P. Degiovanni, S. Olivares, N. Samantaray, P. Traina, and M. Genovese, One and two-mode squeezed light in correlated interferometry, *Phys. Rev. A* **92**, 053821 (2015).
- [58] G. Brida, L. Caspani, A. Gatti, M. Genovese, A. Meda, and I. Ruo-Berchera, Measurement of Sub-Shot-Noise Spatial Correlations without Background Subtraction, *Phys. Rev. Lett.* **102**, 213602 (2009).